Journal of Analytical Science and Technology

RESEARCH ARTICLE Open Access

Laser desorption/ionization mass spectrometry of L-thyroxine (T_4) using combi-matrix of α-cyano-4-hydroxycinnamic acid (CHCA) and graphene

Joo-Yoon Noh[1], Moon-Ju Kim[1], Jong-Min Park[1], Tae-Gyeong Yun[1], Min-Jung Kang[2] and Jae-Chul Pyun[1*]

Abstract

An optimal combi-matrix for MALDI-TOF mass spectrometry was presented for the analysis of L-thyroxine (T_4) in human serum. For the selection of the optimal combi-matrix, several kinds of combi-matrices were prepared by mixing the conventional organic matrix of CHCA with nanomaterials, such as graphene, carbon nanotubes, nanoparticles of Pt and TiO_2. In order to select the optimal combi-matrix, the absorption at the wavelength of laser radiation (337 nm) for the ionization of sample was estimated using UV–Vis spectrometry. And, the heat absorption properties of these combi-matrices were also analyzed using differential scanning calorimetry (DSC), such as onset temperature and fusion enthalpy. In the case of the combi-matrix of CHCA and graphene, the onset temperature and fusion enthalpy were observed to be lower than those of CHCA, which represented the enhanced transfer of heat to the analyte in comparison with CHCA. From the analysis of optical and thermal properties, the combi-matrix of CHCA and graphene was selected to be an optimal combination for the transfer of laser energy during MALDI-TOF mass spectrometry. The feasibility of the combi-matrix composed of CHCA and graphene was demonstrated for the analysis of T_4 molecules using MALDI-TOF mass spectrometry. The combi-matrix of CHCA and graphene was estimated to have an improved limit of detection and a wider detection range in comparison with other kinds of combi-matrices. Finally, the MALDI-TOF MS results of T_4 analysis using combi-matrix were statistically compared with those of the conventional immunoassay.

Keywords: Combi-matrix, Solid matrix, Graphene, Thyroxine, Matrix-assisted laser desorption/ionization time-of-flight mass spectrometry

Introduction

Matrix-assisted laser desorption/ionization time-of-flight mass spectrometry (MALDI-TOF MS) is widely used to analyze biomolecules such as proteins and deoxyribonucleic acid (DNA) with a high molecular weight (Karas and Hillenkamp 1988; Tanaka et al. 1988; Guinan et al. 2015; Lu and Cai 2012). Organic matrices such as α-cyano-4-hydroxycinnamic acid (CHCA) and 2,5-dihydroxybenzoic acid (DHB) are used to absorb the laser radiation in the ultra-violet (UV) range and as proton sources to ionize analytes (Leopold et al. 2018; Bateson et al. 2011). The organic matrices are fragmented during laser energy absorption. These fragments produce mass peaks in the low m/z ratio range of less than 1000 (Kim et al. 2014a; Kim et al. 2013; Park et al. 2015; Park et al. 2017). Because the mass peaks from organic matrices are unreproducible, it is difficult to identify the mass peaks of analytes that occur at low m/z ratios (Noh et al. 2021; Kim, et al. 2021a; Kim, et al. 2021). Therefore, the

*Correspondence: jcpyun@yonsei.ac.kr
[1] Department of Materials Science and Engineering, Yonsei University, 50 Yonsei-ro, Seodaemun-gu, Seoul 03722, Republic of Korea
Full list of author information is available at the end of the article

capability to analyze small molecules is minimal. Organic matrix and analyte formed a crystal with heterogeneous morphology after drying process on a metal plate for MALDI-TOF MS analysis. Depending on the position of the laser radiation, different amounts of analyte ions occur even for the crystals of the same concentration. Thus, the quantitative analysis of small molecules has been restricted by MALDI-TOF MS (Park et al. 2019; Kim et al. 2017; Kim et al. 2020; Choi et al. 2018; Noh et al. 2017).

Matrix selection in MALDI is critical in determining the success or failure of the analysis (Zenobi and Knochenmuss 1998). Various solid matrices composed of inorganic materials have been reported as alternative matrices to solve the problems of the quantitative analysis of small molecules and extend the application range in addition to enhancing the sensitivity of MALDI-TOF MS. These solid matrices are fabricated to produce nanostructures such as nanoparticles (NPs), nanotubes, and nanowires. The solid matrices can be classified according to the base materials: (1) carbon-based nanostructures such as graphene (Banazadeh et al. 2018; Gulbakan et al. 2010; Lu et al. 2011; Chen et al. 2013; Liu et al. 2015; Oh and Biswas 2021), carbon nanotubes (CNTs), and fullerene (Szabo et al. 2010); (2) semiconductor-based nanostructures such as TiO_2 (Kim et al. 2016; Kim et al. 2018; Kim et al. 2019; Kim et al. 2014b; Chen and Chen 2004; Kim and Lee 2021), SnO_2 (Shen, et al. 2010), and CdS (Shrivas and Wu 2010; An et al. 2021); (3) metal-based nanostructures such as Au (Chen et al. 2010; Nayak and Knapp 2010; Kawasaki et al. 2012; Nguyen et al. 2016; Ly and Joo 2014; Li et al. 2012; Kim, et al. 2021b), Pt (Navin et al. 2009), and Ag (Guan et al. 2018). Usually, carbon-based nanostructures can be used as solid matrices because they can absorb laser energy in the UV range and be used as a proton source (Park et al. 2018; Lu et al. 2017). Semiconductor-based nanostructures can also absorb the laser radiation energy and create holes in the valence band and electrons in the conduction band, which can be used to ionize analytes through oxidation and reduction. Metal-based nanostructures can also absorb the laser radiation energy and effectively increase the surface temperature from low thermal conductivity to enhance the ionization of the analyte. Among them, graphene has compelling properties such as strong optical absorption at laser wavelengths, high thermal conductivity (approximately 5000 W mK^{-1}), and fast electron mobility with efficient electron–phonon coupling, making graphene one of the most promising materials for mass spectrometric applications (Balandin et al. 2008; Bolotin et al. 2008; Chung et al. 2013; Kim et al. 2011).

L-thyroxine (T_4) is a thyroid hormone secreted from the thymus that regulates growth and development, carbohydrate metabolism, and protein synthesis (Sinha et al. 2014; Mullur et al. 2014). Monitoring T_4 in human serum and tissues is necessary to assess overall health. For example, a medical diagnosis of congenital hypothyroidism was performed using a cutoff T_4 concentration of approximately 50 ng mL^{-1} (LaFRANCHI 1999; Desai et al. 1994). Clinical laboratories measure the T_4 concentration by radioimmunoassay (RIA), which requires the handling and disposal of radioactive materials (Mizuta et al. 1982; Oberkotter and Tenore 1983; Bong et al. 2021; Jung 2021; Jung et al. 2021). In this study, a new combi-matrix will be presented for the effective ionization of the T_4, which has a low ionization efficiency in MALDI mass analysis. A combi-matrix composed of a conventional CHCA and solid matrix will be presented for the quantitative analysis of T_4. The concept of a combi-matrix is to: (1) enhance the absorption of UV radiation energy and (2) transfer it for the thermal desorption of analytes by mixing solid materials, as shown in Fig. 1a. Ultraviolet-absorbing materials such as CNTs, Pt NPs, and P25 (TiO_2) with high thermal conductivity (Table 1) will be tested as solid matrices to optimize the combi-matrix for the quantitative analysis of T_4, which can effectively absorb the laser radiation to enhance the desorption process (Choi et al. 2018; Banazadeh et al. 2018; Rodríguez et al. 2015; Chen et al. 2016). As shown in Fig. 1b, the mixing of CHCA and a solid matrix changes the ionization efficiency of T_4. The absorption properties of the combi-matrices will be analyzed by wavelength scanning around the UV radiation (337 nm), and the thermal properties to transfer the absorbed energy will be analyzed by differential scanning calorimetry (DSC) to optimize the combi-matrix for T_4 analysis. Quantitative analysis of T_4 will be conducted for T_4 samples in human serum using each combi-matrix.

Materials and methods

Materials

CHCA, DHB, 9-Aminoacridine (9-AA), acetonitrile, 0.1% trifluoroacetic acid (TFA), T_4, methanol, sodium hydroxide, and human serum were purchased from Sigma-Aldrich Co. (St. Louis, MO, USA). Graphene and CNTs were purchased from Enanotec (Sungnam, Korea). P25 TiO_2 nanoparticles were purchased from Evonik Industries AG (Essen, North Rhine-Westphalia, Germany). Platinum NPs were synthesized using the citrate reduction method (Niazov et al. 2007; Duan and Cui 2009; Xu and Cui 2007). Deionized water was obtained from a Milli-Q® water purification system (Millipore, Billerica, MA, USA). Stainless-steel target plates were purchased from Goodfellow Cambridge Ltd. (Huntingdon, Cambridgeshire, UK).

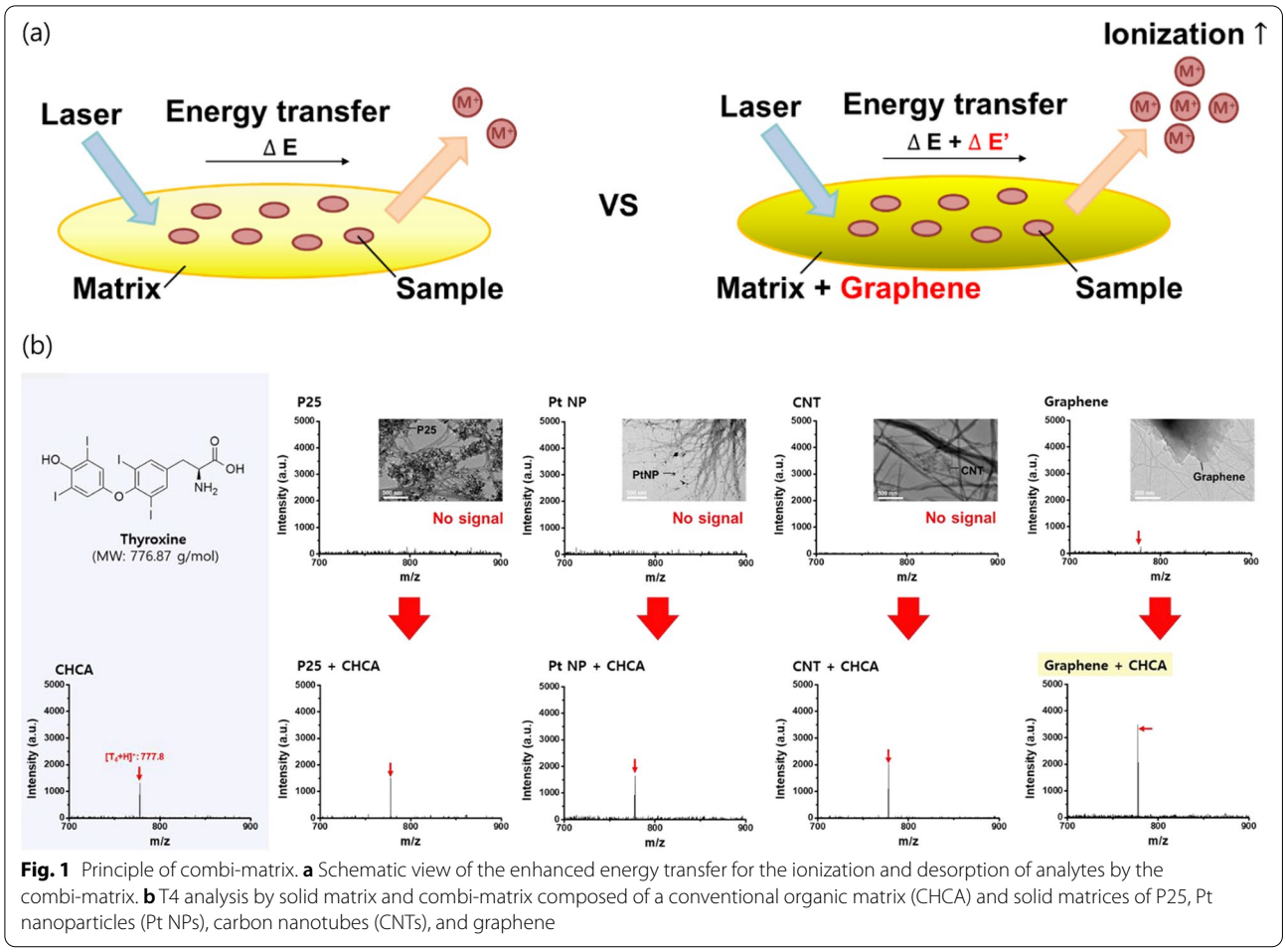

Fig. 1 Principle of combi-matrix. **a** Schematic view of the enhanced energy transfer for the ionization and desorption of analytes by the combi-matrix. **b** T4 analysis by solid matrix and combi-matrix composed of a conventional organic matrix (CHCA) and solid matrices of P25, Pt nanoparticles (Pt NPs), carbon nanotubes (CNTs), and graphene

Table 1 Thermal properties of the solid matrices

	P25	Pt NPs	CNTs	Graphene
Thermal conductivity (W/(m•K))	0.61	100–500	2,400	4,500–5,000
Electron mobility ($cm^2/(V•s)$)	10^{-4}-10^{-5}	10^0	80,000	200,000
Effective surface area (m^2/g)	50	72	380	700

Sample preparation

CHCA was prepared in acetonitrile/0.1% TFA (1:1, v/v) at a concentration of 10 mg mL^{-1}. Graphene and CNTs were prepared at 0.1, 0.5, and 1 mg mL^{-1} in methanol, while P25 was dispersed at 0.1, 0.5, and 1 mg mL^{-1} in deionized water. Standard solutions of T_4 were prepared in 100 μM NaOH/methanol (1:1, v/v), and serial dilutions for T_4 were conducted in the same solvents. Combi-matrix solutions of CHCA and graphene, CNT, P25, and Pt NPs were prepared by mixing the solutions at volume ratios of 1:1. The T_4 sample was premixed with a combi-matrix of CHCA and graphene (1:1 v/v). The mixture (1 μL) was spotted on a stainless-steel target plate and dried for MALDI-TOF MS analysis.

Human serum was spiked with T_4 standard samples to demonstrate the feasibility of diagnosing hypothyroidism. Protein precipitation or extraction was conducted before mass analysis using various organic solvents to precipitate numerous proteins in serum samples (Alshammari et al. 2015). Methanol precipitation was conducted by mixing serum samples (50 μL) with cold methanol (450 μL) and incubating for 20 min. Samples were centrifuged at 12,000 rpm for 10 min at 4 °C, and the supernatant was used for the MALDI-TOF MS analysis. The yield (extraction efficiency) of each protein precipitation method was compared by calculating the recovery at 50 ng mL^{-1} (the cutoff concentration for hypothyroidism).

Characterization of the combi-matrix

The size and distribution of the combi-matrix of CHCA and graphene, CNT, Pt NPs, and P25 were characterized

by using transmission electron microscope (JEM-F200, JEOL, Japan). The optical properties of the combi-matrices were analyzed by using UV/VIS spectrometer (Perkin Elmer, Massachusetts, USA). The thermal properties of the combi-matrices were analyzed through differential scanning calorimeter (PerkinElmer, Massachusetts, USA). The heat flow for CHCA and the combi-matrix was observed in the temperature range of 200–300 °C at an increasing rate of 15 °C/min. Asparagine (Asn, melting temperature of 235 °C) was used as a model heat sink that absorbed the heat flow from the combi-matrix to melt. The thermal properties, onset temperature (T_{onset}), peak temperature (T_{peak}), fusion enthalpy (ΔH_{fus}), and relative thermal conductivity were estimated from the DSC spectrum (Kim et al. 2019).

MALDI-TOF MS analysis

Mass spectrometric analysis of the T_4 standard was conducted using a Voyager DE-STR (AB Sciex, Foster City, CA, USA) equipped with a 337-nm wavelength N_2 laser. The mass spectra were obtained using the positive ion mode with an accelerating voltage of 20 kV and a second ion source voltage of 18 kV. The reflector voltage was set to 9.5 kV, and all mass spectra were obtained by integrating 300 laser pulses for each sample. The signal-to-noise ratio (S/N) was adopted from the equation in the reference (Müller et al. 2001). Ion peaks with S/N larger than three were considered mass signals. The measured intensities for each concentration were plotted as graphs and linearly approximated using the least-squares method. The calculated limit of detection was three times the noise level. The reproducibility of MALDI-TOF MS was verified by inter- and intra-spot analyses of T_4 at a concentration of 200 ng mL^{-1}. Inter-spot analysis was performed at five different sample spots of T_4, and the measurement was taken using the partial random walk function. Intra-spot analysis was also conducted at the same sample spot of T_4 through five rounds of repeated measurements using the partial random walk function.

Statistical analysis

MedCalc software for Windows version 18.6 (Ostend, West Flanders, Belgium) was used for all statistical analyses. The MALDI-TOF MS data were expressed as the mean ± standard deviation. The Mann–Whitney unpaired test was used to examine differences between the MALDI-TOF MS data of only CHCA and the combi-matrices of CHCA and graphene, CNTs, Pt NPs, and P25. A conventional immunoassay was performed as a reference method to analyze free T_4 in the serum at different concentrations using a commercially available ELISA kit for free T_4 from Wkea (Changchun, Jilin, China). The Bland–Altman plot and Passing–Bablok regression were employed to confirm the coincidence of the two analysis methods of MALDI-TOF MS based on the combi-matrix and immunoassay.

Results and discussion

Properties of combi-matrix

The concept of a combi-matrix was (1) to enhance the absorption of UV radiation energy and (2) to transfer it for the thermal desorption of analytes by mixing solid materials, as shown in Fig. 1a. The organic matrix of CHCA is mixed with carbon-based nanostructures of graphene, CNTs, Pt, and P25 with high thermal conductivity to prepare the combi-matrix, as summarized in Table 1. First, the solid matrices of graphene, CNT, Pt NPs, and P25 were utilized to ionize T_4 molecules without any organic matrix. For the comparison of mass peaks, the concentration of solid matrices was set at 0.5 mg mL^{-1}, and the same amount of solid matrix was used by dropping the same volume (1 μL, the absolute amount of 500 ng) for analyzing T_4. As shown in Fig. 1b, the intensity of the mass peak (S/N ratio) of the T_4 molecule (at a concentration of 200 ng mL^{-1}) was 237.5 (2.7), no signal (−0.5), 5.2 (−0.4), and 19.9 (−0.2) for graphene, CNTs, Pt NPs, and P25, respectively. Under similar conditions, the mass peak from the analysis using CHCA was 1248.5 (16.5). The results suggested that the intensity of the mass peak was significantly lower than that of CHCA when only solid matrices were used for ionizing T_4 molecules. After mixing CHCA with the solid matrices, the intensity of the mass peaks (S/N ratio) of T_4 molecules was 3341.8 (45.0), 2093.8 (28.0), 1650.6 (23.6), and 1513.8 (24.5) for graphene, CNTs, Pt NPs, and P25, respectively. The results indicated that the mass intensity and the S/N ratio were significantly increased after mixing CHCA with solid matrices of graphene, CNTs, Pt NPs, and P25. Furthermore, the mass peaks of the combi-matrices consisting of CHCA and solid matrices of graphene, CNTs, P25, and Pt NPs were higher than those of the conventional organic matrix of CHCA. Additionally, the mass peak intensity of different combi-matrices coincided with the order of thermal conductivity and the effective surface area of used solid matrices, as summarized in Table 1 (Grinou et al. 2012; Choo et al. 2012; Kim and Park 2007; Sikdar et al. 2011). Combi-matrix of graphene and graphene showed the highest mass intensity, as graphene showed the highest thermal conductivity (4500–5000 W/(m K)), electron mobility (200,000 cm^2/(V s)), and effective surface area (700 m^2/g) among the solid matrices. Thus, the concept of a combi-matrix: (1) to enhance the absorption of UV radiation energy and (2) to transfer it for the thermal desorption of analytes by mixing solid materials was feasible.

The optical properties before and after mixing the solid matrices with CHCA were analyzed by UV/Vis spectrometry to estimate the enhancement of the absorption of UV radiation energy. As shown in Fig. 2a, CHCA and graphene have maximum absorptions at wavelengths (λ_{max}) of 350 and 270 nm, respectively, which was also reported in previous studies (Robinson et al. 2017; Low et al. 2004; Uran et al. 2017). When graphene was mixed with CHCA, the maximum absorption was observed at a wavelength (λ_{max}) of approximately 285 nm; the absorption increased at a wavelength of 337 nm of the laser radiation for the ionization of the sample. As the turbidity of graphene and the mixture of CHCA and graphene were controlled to be the same at a wavelength of 500 nm, the amount of graphene was similar before and after mixing with CHCA. However, the absorption at wavelengths less than 350 nm was significantly higher than that of graphene before mixing with CHCA. These results indicated that the absorption of the combi-matrix achieved a significantly increased absorption of laser radiation for the effective ionization of T_4 molecules. The combi-matrix of DHB and graphene demonstrated an identical trend of increased absorbance of laser radiation at a wavelength of 337 nm, as shown in Fig. 2b. The UV/Vis spectra of 9-AA showed two broad peaks in the wavelength range of 200 to 500 nm. The absorbance at 337 nm increased when graphene was mixed with 9-AA matrix, as shown in Fig. 2c. Compared with the UV/VIS spectra, the enhancement of absorption of laser radiation at the wavelength of 337 nm was estimated to increase by 9.7%, 7.1%, 6.1%, and 3.1% for graphene, CNTs, Pt NPs, and P25, respectively (Additional file 1: Fig. S1). The results suggested that the combi-matrix enhanced the absorption of UV radiation energy during MALDI-TOF MS, and graphene was the optimal solid matrix for the combi-matrix formation.

Next, the enhancement of the thermal properties of the combi-matrix for the transfer of laser radiation energy was estimated using DSC. The T_{onset}, T_{peak}, and ΔH_{fus} are estimated from the DSC spectrum through the measurement of heat flow in the controlled temperature range to analyze the heat absorption property, as shown in Fig. 3a. The heat flow was observed for CHCA and the combi-matrix of CHCA and graphene in the temperature range of 200–300 °C at an increasing rate of 15 °C/min, and Asn was used as a model heat sink to absorb the heat flow from the combi-matrix to melt. From the slope of the DSC heat flow curve, the relative thermal conductivity was estimated, representing the amount of heat flow required at the phase change of the heat sink.

The DSC spectra were measured for Asn only, Asn with graphene, Asn with CHCA, and Asn with combi-matrix composed of CHCA and graphene. As shown in Fig. 3b, the (ΔH_{fus}) of Asn significantly decreases compared to Asn only, Asn with graphene, and Asn with CHCA. The results implied that Asn melted with a lower heat flow by mixing the organic matrix (CHCA) with a solid graphene matrix. Additionally, from comparing the slope of the DSC spectra, the combi-matrix had a lower relative thermal conductivity than other conditions, indicating a more effective transfer of thermal energy to the heat sink material. The same DSC measurements are taken using DHB and 9-AA as organic matrices of the combi-matrix, as shown in Fig. 3c and Fig. 3d. For the two organic matrices, the ΔH_{fus} of Asn and the relative thermal conductivity from the slope of the DSC spectrum were significantly reduced by mixing graphene compared to those of Asn only, Asn with graphene, and Asn with organic matrix. Thus, the combi-matrix composed of the conventional organic matrix and graphene transferred the energy from UV radiation, which effectively transferred to the analyte for MALDI-TOF MS.

When three different kinds of organic matrices are mixed with graphene, the ΔH_{fus} of Asn and the relative thermal conductivity are minimum for the organic matrix of CHCA, as shown in Fig. 3e and f. These results indicated that the optimal combi-matrix was composed by mixing the conventional organic matrix of CHCA and graphene for the energy transfer from UV radiation for MALDI-TOF MS.

The combination of the solid matrix of graphene and the organic matrices of CHCA, DHB, and 9-AA was also applied for the MALDI-TOF MS of Asn. For the MALDI-TOF MS, the Asn sample at a concentration of 100 μg mL^{-1} was dropped to the combi-matrices of organic matrix and graphene. The mass peak of Asn was observed at the m/z ratio of $[Asn+H]^+ = 133.1$ [reflective positive (RP) mode] and $[Asn\text{-}H]^- = 131.1$ [reflective negative (RN) mode]. When graphene is mixed with the organic matrix of CHCA, the mass peak of Asn has a significantly high S/N ratio of 4.9, comparison to Asn only (S/N ratio of 0.5), Asn with graphene (0.7), and Asn with CHCA (2.7), as shown in Fig. 4a. Furthermore, when DHB and 9-AA were used as the organic matrix of the combi-matrix with graphene, the S/N ratio was significantly higher than Asn only, Asn with graphene, and Asn with organic matrix. The S/N ratio of the mass peak of Asn was 4.9 for CHCA (Fig. 4a), 3.3 for DHB (Fig. 4b), and 3.3 for 9-AA (in RN mode, Fig. 4c) when the mass peak of Asn from the combi-matrices of different organic matrices. From the previous results, the optimal combi-matrix was composed by mixing the conventional organic matrix of CHCA and graphene to absorb the laser energy from the UV/Vis spectrum and the transfer of energy from DSC analysis. These results confirmed that the combi-matrix with graphene and CHCA enhanced the

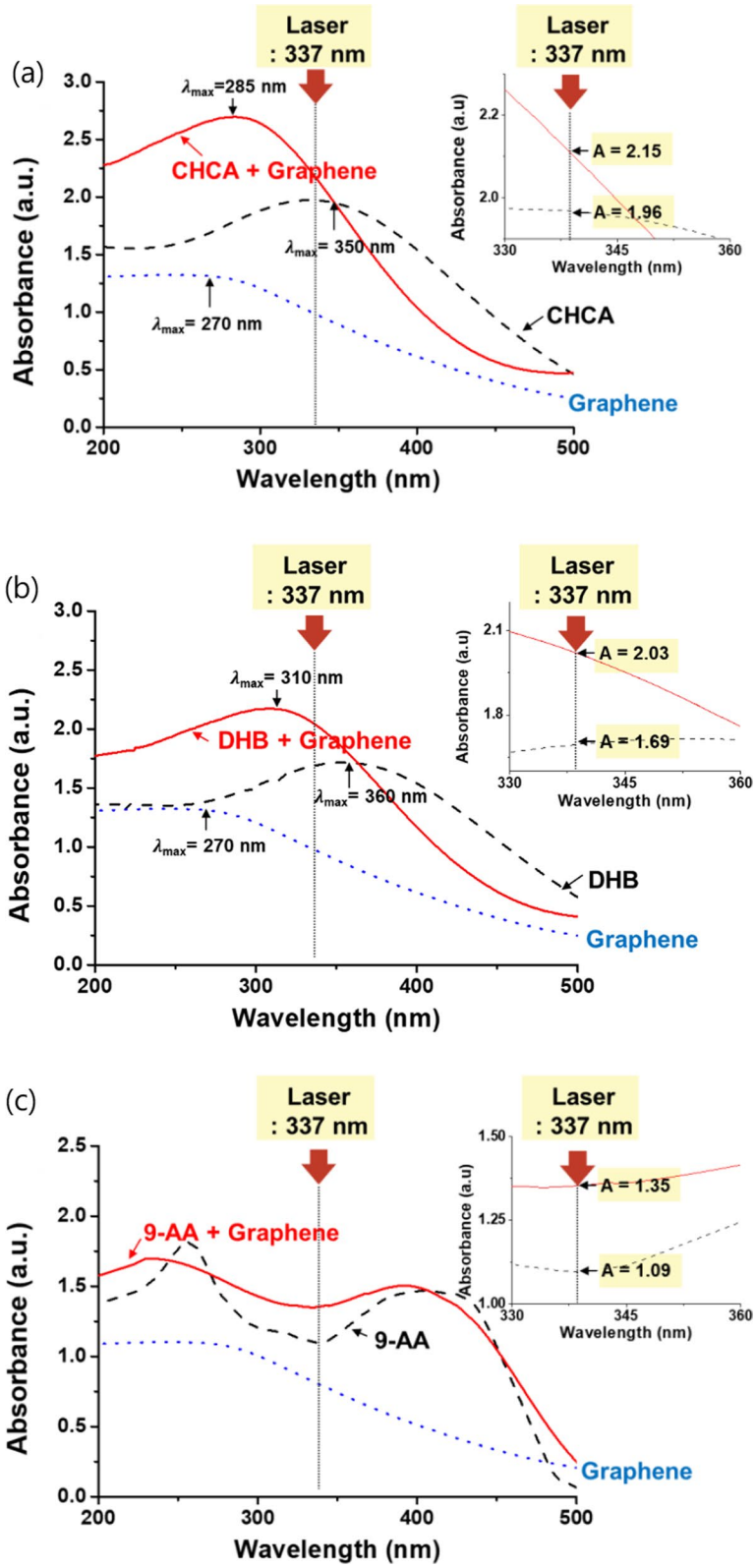

Fig. 2 Optical absorption in the UV range for the combi-matrices composed of the solid matrix (graphene) and the conventional organic matrices of **a** alpha-cyano-4-hydroxycinnamic acid (CHCA), **b** 2,5-dihydroxybenzoic acid (DHB), and **c** 9-AA

absorption of UV radiation energy and the transfer of laser energy during MALDI-TOF MS analysis.

Analysis of L-thyroxine (T_4) using the combi-matrix

The combination of the solid matrix of graphene and the organic matrices of CHCA, DHB, and 9-AA was also applied for MALDI-TOF MS of T_4. For the MALDI-TOF MS, the T_4 sample at a concentration of 200 ng mL^{-1} was dropped on the combi-matrices of the organic matrix and graphene. The mass peak of T_4 was observed at the m/z ratio of $[T_4+H]^+ = 777.8$ (RP mode) and $[T_4—H]^- = 775.8$ (RN mode). When graphene was mixed with the organic matrix of CHCA, the mass peak of T_4 had a significantly higher S/N ratio of 20.6 than T_4 only (S/N ratio of −0.1), T_4 with graphene (0.8), and T_4 with CHCA (7.8). For the mass peak of T_4 from the combi-matrices of different organic matrices, the S/N ratio of the Asn mass peak was 20.6 CHCA [Fig. 5a], 18.9 for DHB [Fig. 5b], and 1.6 for 9-AA [in RP mode, Fig. 5c]. These results confirmed that the combi-matrix with graphene and CHCA was optimal for MALDI-TOF MS.

Quantitative analysis of T_4 molecules was performed using a combi-matrix organic matrix (CHCA) and a solid matrix (graphene). The inhomogeneous co-crystallization of the matrix analyte made quantitative analysis difficult, and the feasibility of the quantitative analysis of T_4 was demonstrated by investigating the reproducibility of the inter- and intra-spot measurements. Five different sample spots are independently detected, as shown in Additional file 1: Fig. S2a and Fig. 6a to measure the inter-spot reproducibility. Based on the analysis of the mass spectra, the inter-spot reproducibility was 6.7% for T_4 (200 ng mL^{-1}). MALDI-TOF mass spectra were obtained at five different positions in one sample spot to estimate the intra-spot reproducibility, as shown in Additional file 1: Fig. S2b and Fig. 6b. Based on the mass spectra, the intra-spot reproducibility was 4.6% for T_4 (200 ng mL^{-1}). Therefore, the analysis of T_4 molecules was conducted with high inter- and intra-spot reproducibility using MALDI-TOF MS based on the combi-matrix of organic matrix and solid matrix.

A combi-matrix consisting of CHCA and graphene was used for quantitative analysis of the T_4 molecules. T_4 samples at the concentration range of 12.5–200 ng mL^{-1} were prepared by considering the cutoff concentration of 50 ng mL^{-1} for the diagnosis of congenital hypothyroidism (Desai et al. 1994), as shown in Fig. 6c. The standard curve for analyzing T_4 molecules was prepared from the repeated measurement and the mass peak, demonstrating high linearity ($r^2 = 0.971$) at the corresponding concentration range. Therefore, the quantitative analysis of T_4 was feasible with high linearity in the concentration range, including the cutoff concentration of 50 ng mL^{-1}, for diagnosing congenital hypothyroidism.

The combi-matrix consisting of CHCA and solid matrices of graphene, CNTs, Pt NPs, and P25 was compared for the quantitative analysis of T_4 molecules at the concentration range of 12.5–200 ng mL^{-1} (Additional file 1: Fig. S3). Figure 6d shows the test results with four different combi-matrices from the quantitative analysis of T_4 molecules. The combi-matrix of CHCA and graphene had the widest intensity range than the conventional organic matrix of CHCA and other combi-matrices. From the statistical analysis (Mann–Whitney unpaired test), the test results between the organic matrix of CHCA and the combi-matrices of CHCA and graphene, CNTs, Pt NPs, and P25 were independent, with P-values less than 0.0001. Whiskers show the minimum and maximum values, the boxes represent 25–75% data ranges, horizontal lines within boxes are medians, and diamond symbols are the means of the mass spectrometric results. These results showed that the combi-matrix of CHCA and graphene was effectively used for the quantitative analysis of T_4 molecules in a wider concentration range compared to CHCA and other kinds of combi-matrices. T4 molecules were detectable in the low concentration range (below 75% range) when using CHCA and graphene as a combi-matrix from the box plot.

As shown in Fig. 7a, T_4 samples at a concentration range of 12.5–200 ng mL^{-1} are prepared in human serum after methanol extraction to precipitate proteins, and the extracts of T_4 samples were analyzed using the combi-matrices. When T_4 analysis was performed using only CHCA as a matrix, the mass peak of T_4 was observed at a concentration of more than 100 ng mL^{-1}. When the combi-matrix consisting of CHCA and graphene was used for analyzing T_4, the mass peak of T_4 was observed over the entire concentration range, including the cutoff concentration of 50 ng mL^{-1} for diagnosing congenital hypothyroidism. As shown in Fig. 7(b), the standard curve for analyzing T_4 molecules is obtained from the repeated measurements and the mass peaks, exhibiting high linearity ($r^2 < 0.99$) at the corresponding concentration range. These results indicated that the combi-matrix consisting of CHCA and graphene was used for the quantitative analysis of T_4 samples spiked in serum.

(See figure on next page.)

Fig. 3 Analysis of the thermal properties of the combi-matrix. **a** Schematic view of differential scanning calorimetry (DSC). DSC profiles of the combi-matrix composed of **b** α-cyano-4-hydroxycinnamic acid (CHCA) and graphene, **c** 2,5-dihydroxybenzoic acid (DHB), and graphene, and **d** 9-AA and graphene. The thermal parameters of the onset temperature, peak temperature, enthalpy of fusion, and relative thermal conductivity were estimated from each DSC profile

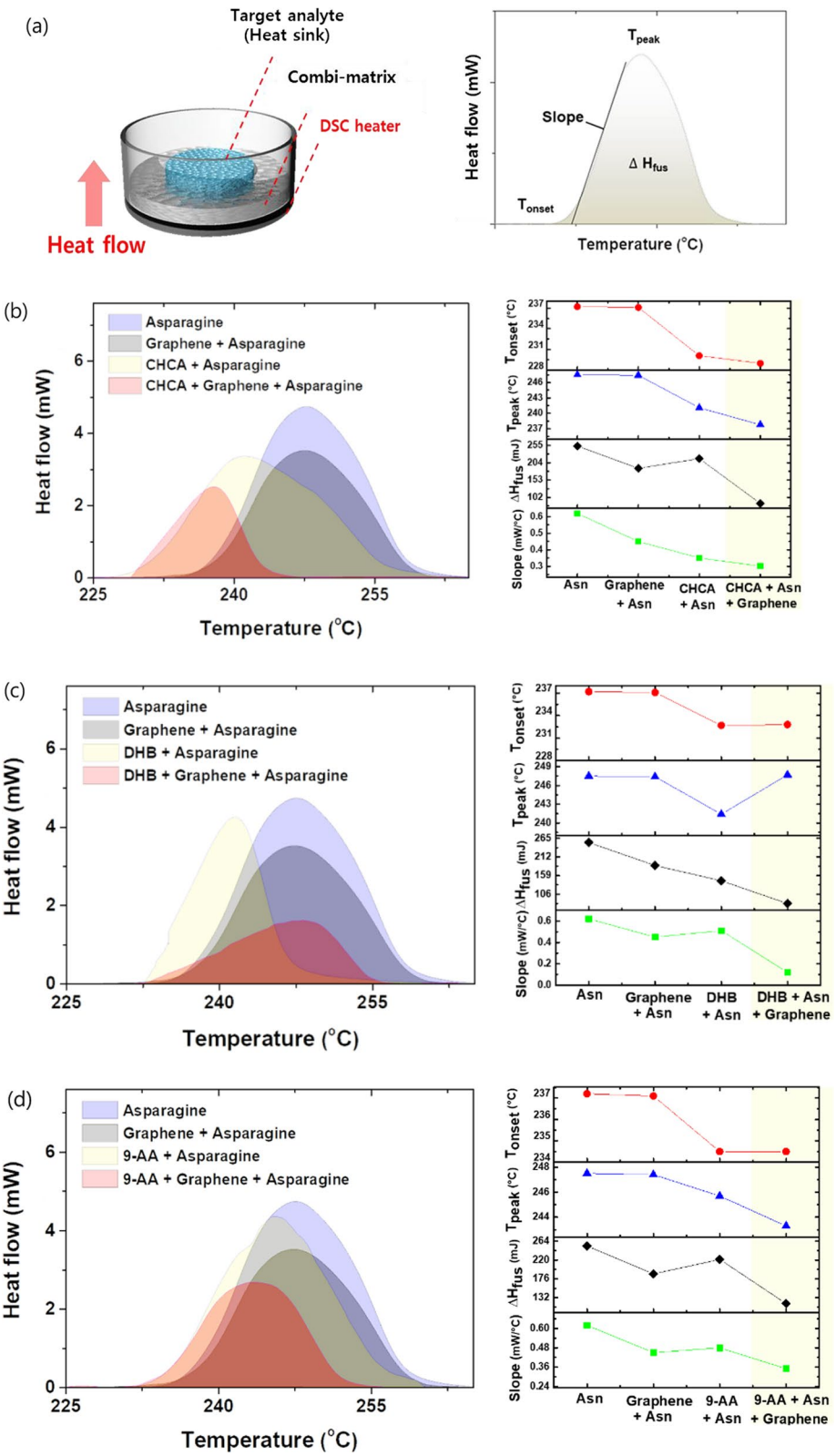

Fig. 3 (See legend on previous page.)

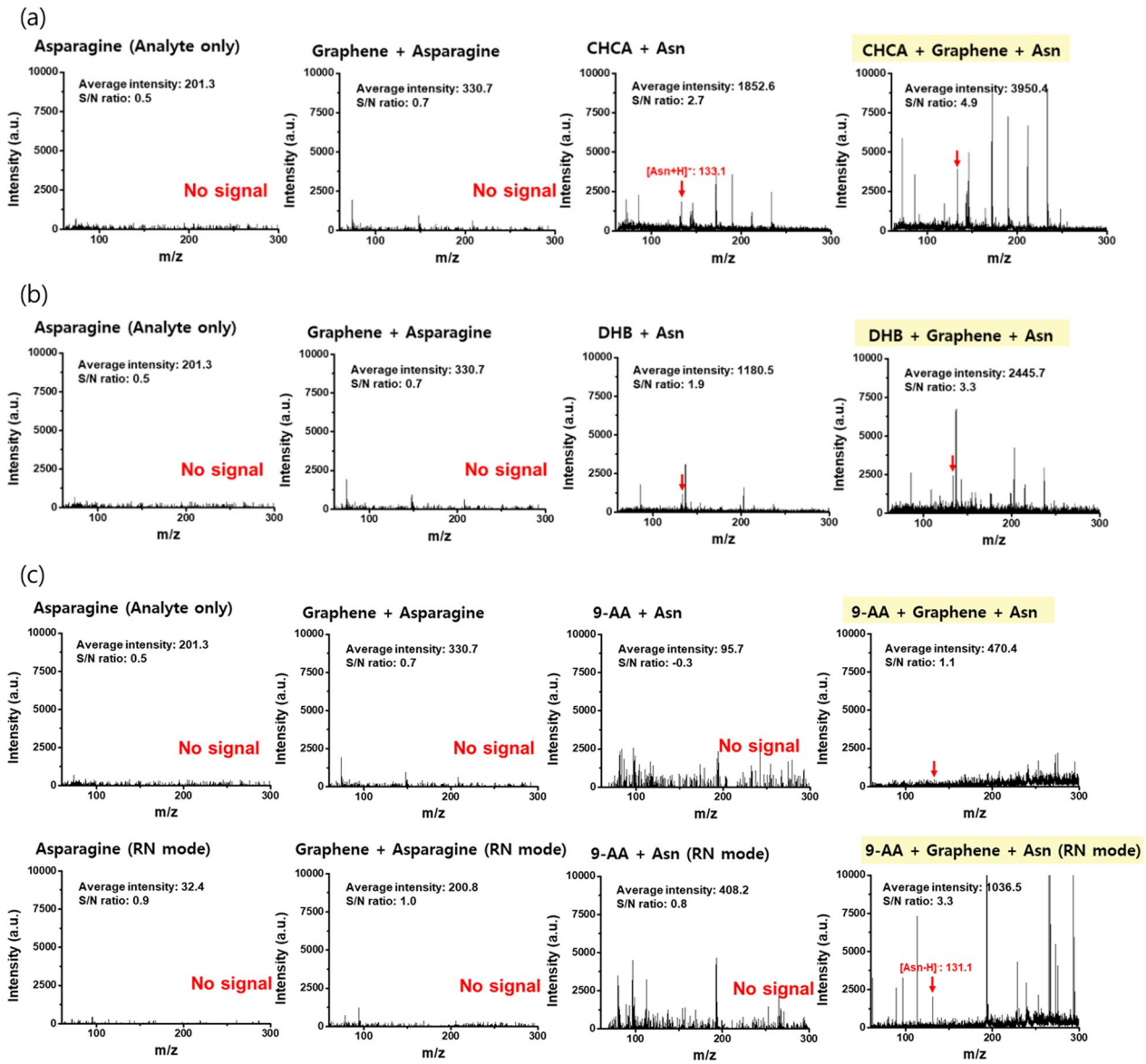

Fig. 4 MALDI-TOF mass spectrometry based on the combi-matrix using Asparagine (Asn) as a model analyte. The combi-matrix was composed of **a** CHCA and graphene, **b** DHB and graphene, and **c** 9-AA and graphene

The box plot shows the test results with four different combi-matrices from the quantitative analysis of T_4 molecules, indicating that the combi-matrix of CHCA and graphene had the widest intensity range than the conventional organic matrix of CHCA and other kinds of combi-matrices [Fig. 7c]. From the statistical analysis (Mann–Whitney unpaired test), the test results between the organic matrix of CHCA and the combi-matrix of CHCA and graphene were independent, with *P*-values of less than 0.0001. These results showed that the combi-matrix of CHCA and graphene could be effectively used for the quantitative analysis of T_4 molecules spiked in serum in a wider concentration range compared to the conventional organic matrix of CHCA.

The clinical laboratories commonly quantify T_4 by RIA, an immunoassay that is complicated to handle and dispose of radioactive materials. In this study, the free T_4 ELISA kit was used as a reference method, and its quantitative analysis results for T_4 were compared to those from MALDI-TOF MS based on the combi-matrix of CHCA and graphene. The Bland–Altman plot and Passing–Bablok regression were conducted using

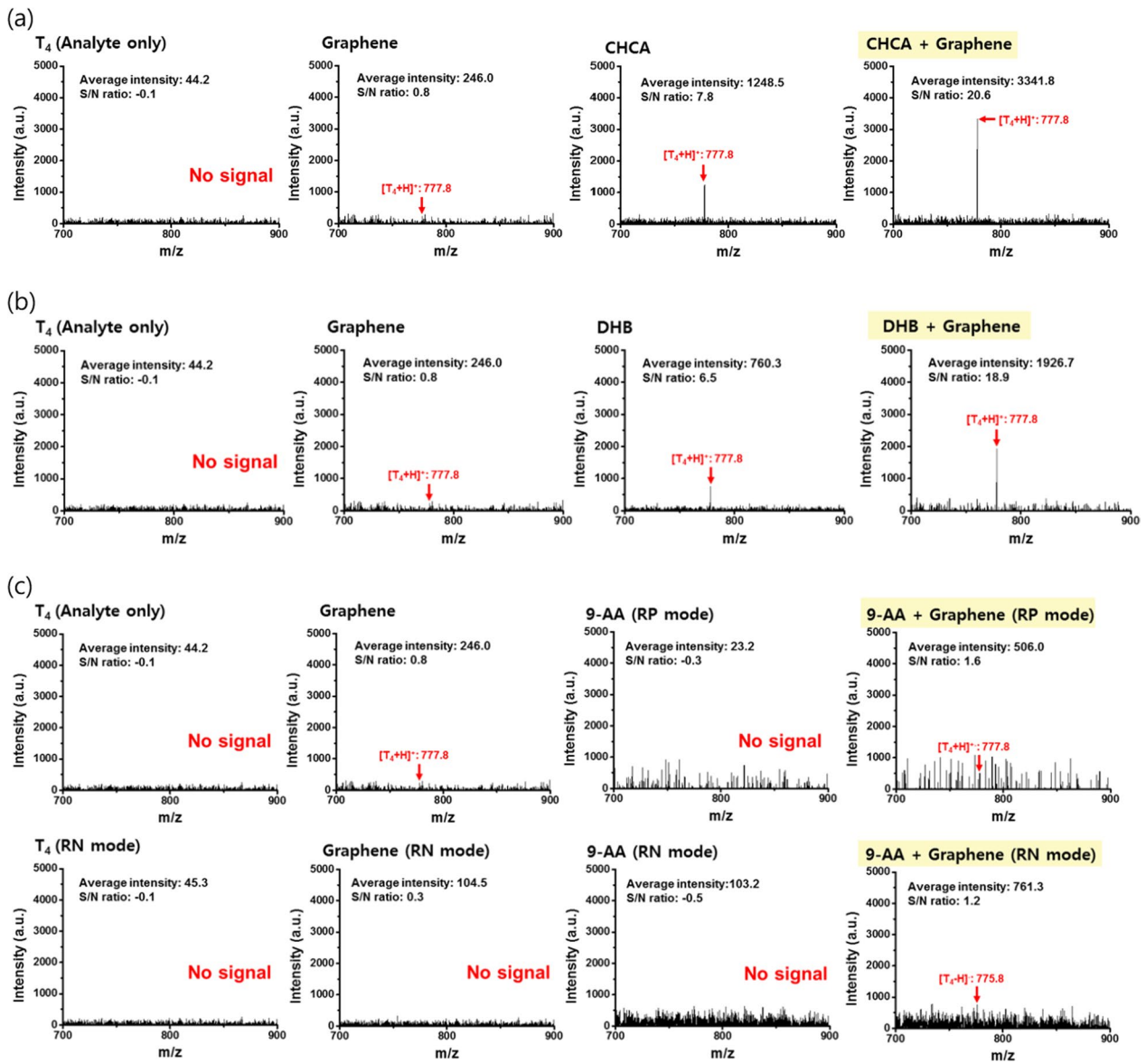

Fig. 5 T4 analysis using MALDI-TOF MS based on the combi-matrix. The combi-matrix was composed of **a** CHCA and graphene, **b** DHB and graphene, and **c** 9-AA and graphene

MedCalc software (version 18.6) to estimate the statistical coincidence of the two methods for T_4 analysis. The Bland–Altman test revealed that a signal difference is distributed within a confidence level of 95% (±1.96 σ), as shown in Fig. 8a. This result demonstrated that the two methods were highly correlated and provided similar analysis results for detecting T_4. In the case of the Passing–Bablok regression, the signals from one method were plotted against the other method when the signals of the two methods had a linear correlation. The analysis data from both methods are distributed at a confidence level of 95%, with a Spearman correlation coefficient (ρ) of 0.973 ($p < 0.0001$), as shown in Fig. 8b. These results indicated that the two different methods were statistically and highly coincident. Moreover, the two methods were highly correlated and provided similar analysis results for detecting T_4.

Conclusion

The organic matrix of CHCA was mixed with carbon-based nanostructures of graphene, CNTs, Pt NPs, and P25 for preparing the combi-matrix. The optical

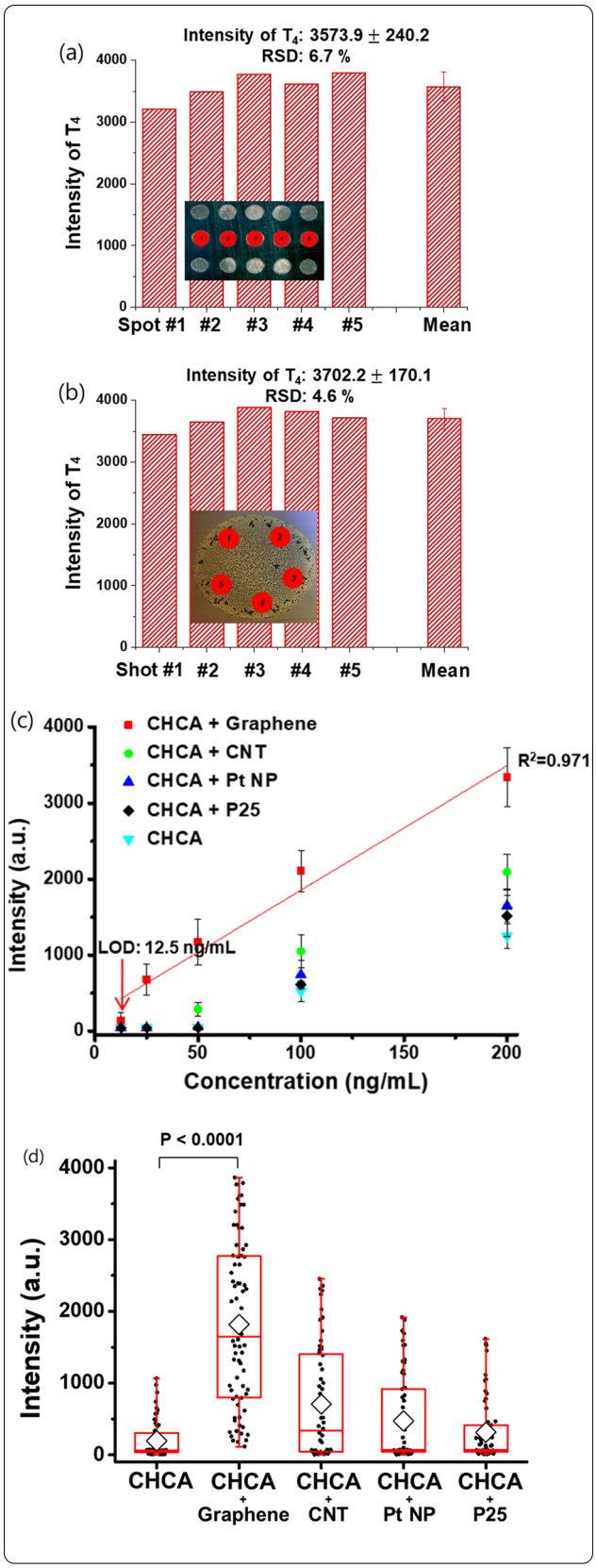

Fig. 6 Quantitative analysis of T4 in buffer using MALDI-TOF MS based on the combi-matrix. **a** Spot-to-spot reproducibility. **b** Shot-to-shot reproducibility. **c** Standard curves for analyzing T4 using MALDI-TOF MS based on the combi-matrices. **d** The Mann–Whitney test T4 analysis using MALDI-TOF MS based on the four different kinds of combi-matrices

properties changed after mixing the solid matrices with CHCA, which were analyzed through UV/VIS spectrometry. The maximum absorption was observed at a wavelength (λ_{max}) of approximately 260 nm when graphene was mixed with CHCA. The absorption increased at a wavelength of 337 nm of the laser radiation for the ionization of the sample. The results suggested that the absorption of the combi-matrix can achieve a significantly increased absorption of laser radiation for the effective ionization of T_4 molecules. The onset temperature and fusion enthalpy were estimated for analyzing the heat absorption property through DSC. In the case of the combi-matrix, the onset temperature and fusion enthalpy were lower than those of CHCA. These results indicate that the combi-matrix can increase the temperature using a smaller amount of heat than CHCA. The analysis of T_4 molecules could be detected with high inter- and intra-spot reproducibility (within 10% RSD) using MALDI-TOF MS based on the combi-matrix of organic matrix and solid matrix. The combi-matrices consisting of CHCA and solid matrices of graphene were used for the quantitative analysis of T_4 molecules spiked in serum after methanol extraction. The standard curve for the analysis of T_4 molecules was prepared from the repeated measurements and the mass peaks, demonstrating high linearity ($r^2 < 0.97$) at the corresponding concentration range. These results suggest that the combi-matrix consisting of CHCA and graphene can be used for the quantitative analysis of T_4 samples spiked in serum. From the statistical analysis (Mann–Whitney unpaired test), the test results between the organic matrix of CHCA and the combi-matrix of CHCA and graphene were independent with P-values of less than 0.0001. Thus, the combi-matrix of CHCA and graphene can be effectively used for the quantitative analysis of T_4 molecules spiked in serum in a significantly wider concentration range than the conventional organic matrix of CHCA. Finally, the T_4 analysis results with the combi-matrix were statistically compared with those of the conventional immunoassay.

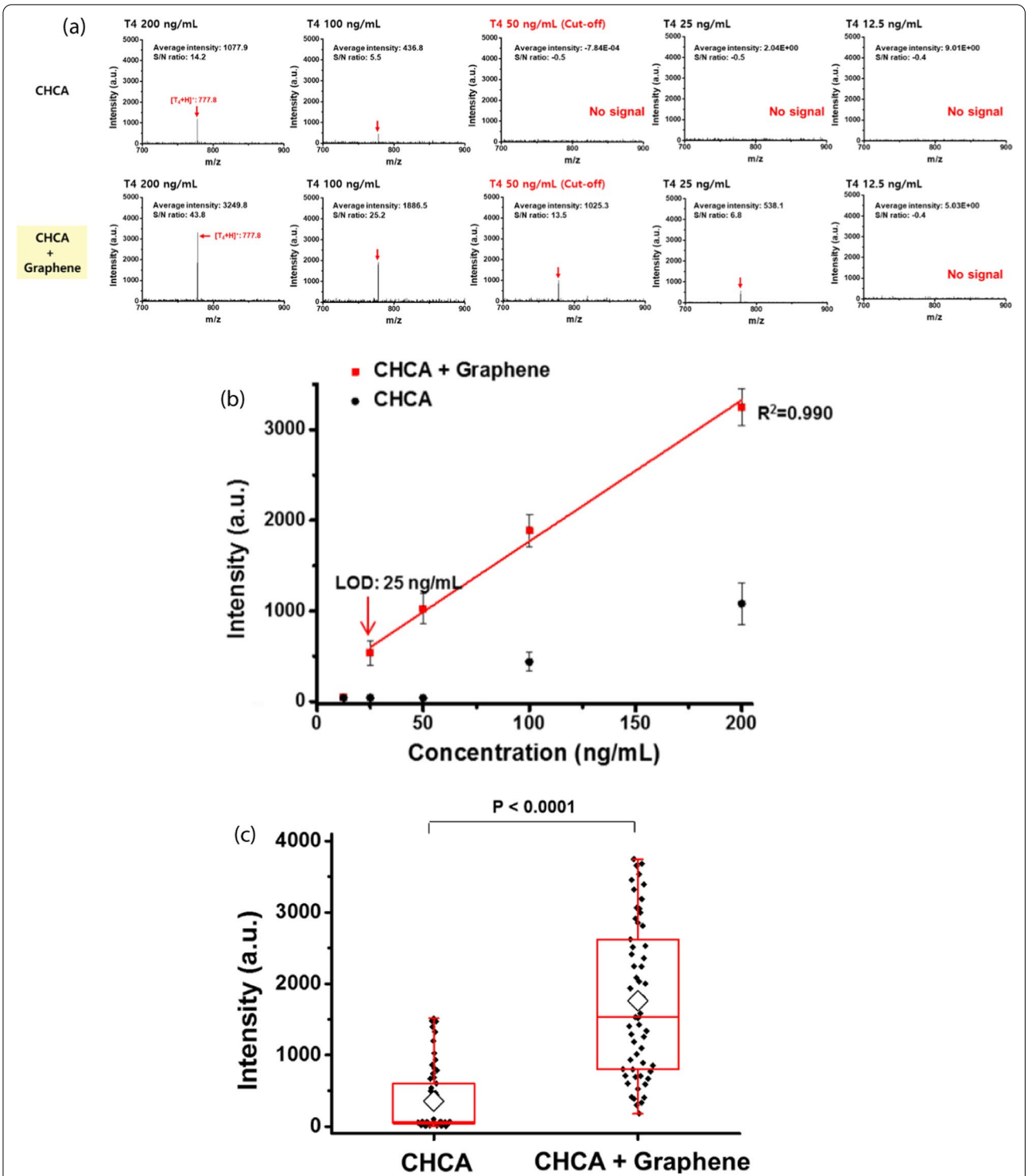

Fig. 7 Quantitative analysis of T4 spiked in serum using MALDI-TOF MS based on the combi-matrix. **a** Spectra of MALDI-TOF MS based on the combi-matrix composed of alpha-cyano-4-hydroxycinnamic acid (CHCA) and graphene. **b** Standard curves for the analysis of T4 using MALDI-TOF MS based on the combi-matrix composed of CHCA and graphene. **c** The Mann–Whitney test T4 analysis using MALDI-TOF MS based on the combi-matrix composed of CHCA and graphene

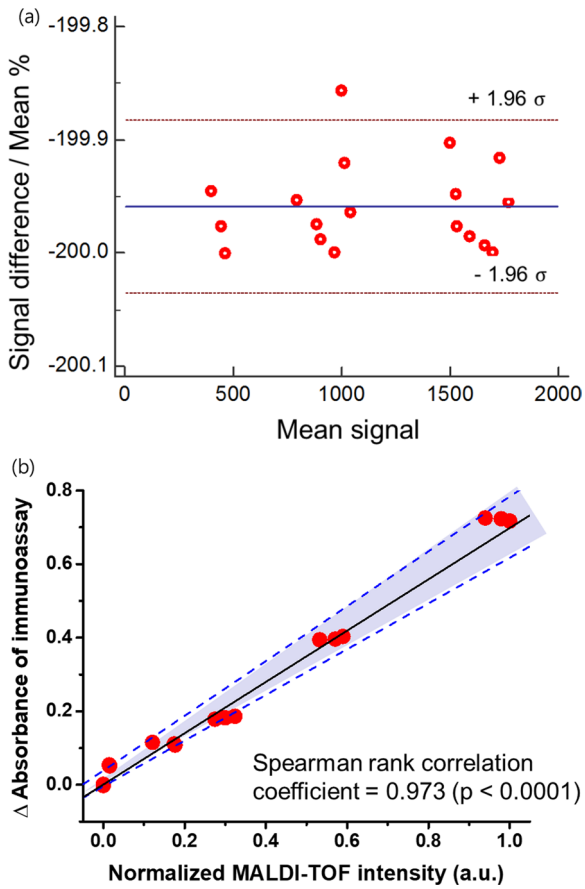

Fig. 8 Statistical analysis between the conventional immunoassay and MALDI-TOF MS based on the combi-matrix for the quantitative analysis of T4. **a** The Bland–Altman test. **b** The Passing–Bablok regression

Abbreviations

Asn: Asparagine; CHCA: α-Cyano-4-hydroxycinnamic acid; CNT: Carbon nanotube; NP: Nanoparticle; TEM: Transmission electron microscopy; DSC: Differential scanning calorimetry; RIA: Radioimmunoassay; RN: Reflective negative; RP: Reflective positive; S/N: Signal-to-noise ratio.

Supplementary Information

The online version contains supplementary material available at https://doi.org/10.1186/s40543-022-00314-9.

Additional file 1: Fig. S1. Optical absorption in the UV range of a combi-matrix composed of an organic matrix (CHCA) to the solid matrices of (a) CNTs, (b) Pt NPs, and (c) P25 (TiO_2). **Fig. S2**. Reproducibility of the combi-matrix of α-cyano-4-hydroxycinnamic acid (CHCA) and graphene for T4 analysis. Mass spectra of (a) spot-to-spot reproducibility of T_4 and shot-to-shot reproducibility of T_4. **Fig. S3**. Mass spectra of quantitative analysis of T_4 in buffer using MALDI-TOF MS based on a combi-matrix.

Acknowledgements

"Not applicable".

Authors' contributions

J-YN performed experiment, data curation, writing–original draft. M-JK, J-MP, and TGY contributed to experiment and data curation. M-JK: done supervision, review & editing. J-CP was involved in supervision, funding acquisition, writing–original draft, review and editing. All authors read and approved the final manuscript.

Funding

This work was supported by the National Research Foundation of Korea [grant numbers: NRF-2020R1A2B5B01002187, NRF-2020R1A5A101913111, and NRF-2021R1A2C209370611].

Declarations

Competing interests

No competing interests related to this paper.

Author details

[1]Department of Materials Science and Engineering, Yonsei University, 50 Yonsei-ro, Seodaemun-gu, Seoul 03722, Republic of Korea. [2]Korea Institute of Science and Technology (KIST), 5 Hwarang-ro 14-gil, Seongbuk-gu, Seoul 02792, Republic of Korea.

Received: 5 December 2021 Accepted: 17 January 2022
Published online: 03 February 2022

References

Alshammari TM, et al. Comparison of different serum sample extraction methods and their suitability for mass spectrometry analysis. Saudi Pharmaceutical J. 2015;23(6):689–97.
An B-G, et al. Photosensors-based on cadmium sulfide (CdS) nanostructures: a review. J Korean Ceram Soc. 2021;58(6):631–44.
Balandin AA, et al. Superior thermal conductivity of single-layer graphene. Nano Lett. 2008;8(3):902–7.
Banazadeh A, et al. Carbon nanoparticles and graphene nanosheets as MALDI matrices in glycomics: a new approach to improve glycan profiling in biological samples. J Am Soc Mass Spectrom. 2018;29(9):1892–900.
Bateson H, et al. Use of matrix-assisted laser desorption/ionisation mass spectrometry in cancer research. J Pharmacol Toxicol Methods. 2011;64(3):197–206.
Bolotin KI, et al. Ultrahigh electron mobility in suspended graphene. Solid State Commun. 2008;146(9–10):351–5.
Bong J-H, et al. Competitive immunoassay of SARS-CoV-2 using pig sera-derived anti-SARS-CoV-2 antibodies. BioChip J. 2021;15(1):100–8.
Chen CT, Chen YC. Desorption/ionization mass spectrometry on nanocrystalline titania sol–gel-deposited films. Rapid Commun Mass Spectrom. 2004;18(17):1956–64.
Chen W-T, et al. Quantification of captopril in urine through surface-assisted laser desorption/ionization mass spectrometry using 4-mercaptobenzoic acid-capped gold nanoparticles as an internal standard. J Am Soc Mass Spectrom. 2010;21(5):864–7.
Chen S, et al. Carbon nanodots as a matrix for the analysis of low-molecular-weight molecules in both positive-and negative-ion matrix-assisted laser desorption/ionization time-of-flight mass spectrometry and quantification of glucose and uric acid in real samples. Anal Chem. 2013;85(14):6646–52.
Chen Y, et al. Carbon dots and 9AA as a binary matrix for the detection of small molecules by matrix-assisted laser desorption/ionization mass spectrometry. J Am Soc Mass Spectrom. 2016;27(7):1227–35.
Choi YK, Oh JY, Han SY. Large-area graphene films as target surfaces for highly reproducible matrix-assisted laser desorption ionization suitable for quantitative mass spectrometry. J Am Soc Mass Spectrom. 2018;29(10):2003–11.
Choo H, et al. Fabrication and applications of carbon nanotube fibers. Carbon Lett. 2012;13(4):191–204.

Chung C, et al. Biomedical applications of graphene and graphene oxide. Acc Chem Res. 2013;46(10):2211–24.
Desai M, et al. Neonatal screening for congenital hypothyroidism using the filter paper thyroxine technique. Indian J Med Res. 1994;100:36–42.
Duan C-F, Cui H. Time-tunable autocatalytic lucigenin chemiluminescence initiated by platinum nanoparticles and ethanol. Chem Commun. 2009;18:2574–6.
Grinou A, et al. Dispersion of Pt nanoparticle-doped reduced graphene oxide using aniline as a stabilizer. Materials. 2012;5(12):2927–36.
Guan M, et al. Silver nanoparticles as matrix for MALDI FTICR MS profiling and imaging of diverse lipids in brain. Talanta. 2018;179:624–31.
Guinan T, et al. Surface-assisted laser desorption ionization mass spectrometry techniques for application in forensics. Mass Spectrom Rev. 2015;34(6):627–40.
Gulbakan B, et al. A dual platform for selective analyte enrichment and ionization in mass spectrometry using aptamer-conjugated graphene oxide. J Am Chem Soc. 2010;132(49):17408–10.
Jung J, et al. Isolation of antibodies against the spike protein of SARS-CoV from pig serum for competitive immunoassay. BioChip J. 2021;15(4):396–405.
Jung J et al (2021) Anti-SARS-CoV-2 nucleoprotein antibodies derived from pig serum with a controlled specificity. Biochip J 1–9
Karas M, Hillenkamp F. Laser desorption ionization of proteins with molecular masses exceeding 10,000 daltons. Anal Chem. 1988;60(20):2299–301.
Kawasaki H, et al. Platinum vapor deposition surface-assisted laser desorption/ionization for imaging mass spectrometry of small molecules. Rapid Commun Mass Spectrom. 2012;26(16):1849–58.
Kim S-E, Lee H-S. An electric field-assisted photochemical metal–organic deposition allowing control of oxygen content for resistive switching in directly patterned TiOx films. J Korean Ceram Soc. 2021;58(6):672–8.
Kim S, Park S-J. Preparation and electrochemical behaviors of platinum nanoparticles impregnated on binary carbon supports as catalyst electrodes of direct methanol fuel cells. J Solid State Electrochem. 2007;11(6):821–8.
Kim Y-K, et al. Synergistic effect of graphene oxide/MWCNT films in laser desorption/ionization mass spectrometry of small molecules and tissue imaging. ACS Nano. 2011;5(6):4550–61.
Kim JI, et al. Covalent protein immobilization with a parylene-H film for matrix-assisted laser desorption/ionization time-of-flight mass spectrometry. Rapid Commun Mass Spectrom. 2013;27(10):1149–54.
Kim JI, et al. Parylene-matrix chip for small molecule analysis using matrix-assisted laser desorption/ionization time-of-flight mass spectrometry. Rapid Commun Mass Spectrom. 2014a;28(3):274–80.
Kim JI, et al. Nylon nanoweb with TiO2 nanoparticles as a solid matrix for matrix-assisted laser desorption/ionization time-of-flight mass spectrometry. Rapid Commun Mass Spectrom. 2014b;28(22):2427–36.
Kim J-I, et al. Analysis of benzylpenicillin in milk using MALDI-TOF mass spectrometry with top-down synthesized TiO2 nanowires as the solid matrix. Chemosphere. 2016;143:64–70.
Kim J-I, et al. Newborn screening by matrix-assisted laser desorption/ionization mass spectrometry based on parylene-matrix chip. Anal Biochem. 2017;530:31–9.
Kim M, et al. TiO2 nanowires from wet-corrosion synthesis for peptide sequencing using laser desorption/ionization time-of-flight mass spectrometry. ACS Appl Mater Interfaces. 2018;10(40):33790–802.
Kim M-J, et al. Synergistic effect of the heterostructure of Au nanoislands on TiO2 nanowires for efficient ionization in laser desorption/ionization mass spectrometry. ACS Appl Mater Interfaces. 2019;11(22):20509–20.
Kim M-J, et al. Coffee ring effect free TiO2 nanotube array for quantitative laser desorption/ionization mass spectrometry. ACS Appl Nano Mater. 2020;3(9):9249–59.
Kim MJ, et al. Photothermal structural dynamics of Au nanofurnace for in situ enhancement in desorption and ionization. Small. 2021;17(49):2103745.
Kim, M.J., et al., *Laser-Induced Surface Reconstruction of Nanoporous Au-Modified TiO2 Nanowires for In Situ Performance Enhancement in Desorption and Ionization Mass Spectrometry.* Advanced Functional Materials, 2021: p. 2102475.
Kim MJ et al (2021) Photothermal structural dynamics of Au nanofurnace for in situ enhancement in desorption and ionization. Small 2103745
LaFRANCHI S. Congenital hypothyroidism: etiologies, diagnosis, and management. Thyroid. 1999;9(7):735–40.
Leopold J, et al. Recent developments of useful MALDI matrices for the mass spectrometric characterization of lipids. Biomolecules. 2018;8(4):173.
Li Y, et al. Resonance scattering particles as biological nanosensors in vitro and in vivo. Chem Soc Rev. 2012;41(2):632–42.
Liu Q, et al. Graphene oxide nanoribbons: improved synthesis and application in MALDI mass spectrometry. Chem A Eur J. 2015;21(14):5594–9.
Low W, et al. MALDI-MS analysis of peptides modified with photolabile arylazido groups. J Am Soc Mass Spectrom. 2004;15(8):1156–60.
Lu M, et al. Matrix interference-free method for the analysis of small molecules by using negative ion laser desorption/ionization on graphene flakes. Anal Chem. 2011;83(8):3161–9.
Lu M, et al. Nanomaterials as assisted matrix of laser desorption/ionization time-of-flight mass spectrometry for the analysis of small molecules. Nanomaterials. 2017;7(4):87.
Lu, M. and Z. Cai, *Advances of MALDI-TOF MS in the analysis of traditional Chinese medicines.* Applications of MALDI-TOF Spectroscopy, 2012: p. 143–164.
Ly NH, Joo S-W. Hg (II) Raman sensor of poly-L-lysine conformation change on gold nanoparticles. BioChip J. 2014;8(4):303–9.
Mizuta H, et al. Radioimmunoassay of" free thyroxin" in dried blood spots on filter paper-preliminary observations on the effective differentiation of subjects with congenital hypothyroidism from those with subnormal thyroxin-binding globulin and normal subjects. Clin Chem. 1982;28(3):505–8.
Müller M, et al. Limits for the detection of (poly-) phosphoinositides by matrix-assisted laser desorption and ionization time-of-flight mass spectrometry (MALDI-TOF MS). Chem Phys Lipid. 2001;110(2):151–64.
Mullur R, Liu Y-Y, Brent GA. Thyroid hormone regulation of metabolism. Physiol Rev. 2014;94(2):355–82.
Navin JK, et al. Characterization of colloidal platinum nanoparticles by MALDI-TOF mass spectrometry. Anal Chem. 2009;81(15):6295–9.
Nayak R, Knapp DR. Matrix-free LDI mass spectrometry platform using patterned nanostructured gold thin film. Anal Chem. 2010;82(18):7772–8.
Nguyen NLT, et al. Sensitive detection of lead ions using sodium thiosulfate and surfactant-capped gold nanoparticles. BioChip J. 2016;10(1):65–73.
Niazov T, Shlyahovsky B, Willner I. Photoswitchable electrocatalysis and catalyzed chemiluminescence using photoisomerizable monolayer-functionalized surfaces and Pt nanoparticles. J Am Chem Soc. 2007;129(20):6374–5.
Noh J-Y, et al. Gold nanoislands chip for laser desorption/ionization (LDI) mass spectrometry. BioChip J. 2017;11(3):246–54.
Noh J-Y, et al. Quantitative analysis of galactose using LDI-TOF MS based on a TiO2 nanowire chip. J Anal Sci Technol. 2021;12(1):1–12.
Oberkotter LV, Tenore A. Separation and radioimmunoassay of T3 and T4 in human breast milk. Hormone Res Paediatrics. 1983;17(1):11–8.
Oh W-C, Biswas MRUD (2021) 3D shape of BiVO 4-GO nanocomposite for excellent photocatalytic performance on standard and industrial dyes under visible light. J Korean Ceram Soc 1–10
Park J-M, et al. Highly sensitive bacterial susceptibility test against penicillin using parylene-matrix chip. Biosens Bioelectron. 2015;71:306–12.
Park J-M, et al. Hypersensitive antibiotic susceptibility test based on a β-lactamase assay with a parylene-matrix chip. Enzyme Microb Technol. 2017;97:90–6.
Park J-M, et al. Mass spectrometry based on nanomaterials. Ceramist. 2018;21(3):249–69.
Park J-M, et al. MALDI-TOF mass spectrometry based on parylene-matrix chip for the analysis of lysophosphatidylcholine in sepsis patient sera. Anal Chem. 2019;91(22):14719–27.
Robinson KN, Steven RT, Bunch J. Matrix optical absorption in UV-MALDI MS. J Am Soc Mass Spectrom. 2017;29(3):501–11.
Rodríguez CE, et al. Conventional matrices loaded onto a graphene layer enhances MALDI-TOF/TOF signal: its application to improve detection of phosphorylated peptides. J Am Soc Mass Spectrom. 2015;27(2):366–9.
Shen WW, et al. SnO2@ Poly (HEMA-co-St-co-VPBA) core-shell nanoparticles designed for selectively enriching glycopeptides followed by MALDI-MS analysis. Chem Asian J. 2010;5(5):1185–91.
Shrivas K, Wu HF. Multifunctional nanoparticles composite for MALDI-MS: Cd2+-doped carbon nanotubes with CdS nanoparticles as the matrix, preconcentrating and accelerating probes of microwave enzymatic digestion of peptides and proteins for direct MALDI-MS analysis. J Mass Spectrom. 2010;45(12):1452–60.
Sikdar S, Basu S, Ganguly S. Investigation of electrical conductivity of titanium dioxide nanofluids. Int J Nanoparticles. 2011;4(4):336–49.
Sinha RA, Singh BK, Yen PM. Thyroid hormone regulation of hepatic lipid and carbohydrate metabolism. Trends Endocrinol Metab. 2014;25(10):538–45.

Szabo Z, et al. Laser desorption/ionization mass spectrometric analysis of small molecules using fullerene-derivatized silica as energy-absorbing material. J Mass Spectrom. 2010;45(5):545–52.
Tanaka K, et al. Protein and polymer analyses up to m/z 100 000 by laser ionization time-of-flight mass spectrometry. Rapid Commun Mass Spectrom. 1988;2(8):151–3.
Uran S, Alhani A, Silva C. Study of ultraviolet-visible light absorbance of exfoliated graphite forms. AIP Adv. 2017;7(3):035323.
Xu SL, Cui H. Luminol chemiluminescence catalysed by colloidal platinum nanoparticles. Luminescence J Biol Chem Luminescence. 2007;22(2):77–87.
Zenobi R, Knochenmuss R. Ion formation in MALDI mass spectrometry. Mass Spectrom Rev. 1998;17(5):337–66.

Publisher's Note